PCCP

PAPER

View Article Online
View Journal | View Issue

Cite this: *Phys. Chem. Chem. Phys.*, 2015, **17**, 21533

Density functional theory calculations of the hydrazine decomposition mechanism on the planar and stepped Cu(111) surfaces

Saeedeh S. Tafreshi,[a] Alberto Roldan[ab] and Nora H. de Leeuw*[ab]

We have investigated the adsorption of hydrazine (N_2H_4) and its reactivity on terraces and steps of Cu(111) surfaces by first-principles calculations in order to gain insight into the hydrazine decomposition mechanism. We have investigated different possibilities for the N–N and N–H bond cleavage for any intermediate states by analysing the reaction and barrier energies of each elementary step. We have found that hydrazine dehydrogenation *via* N–H bond scission is neither energetically nor kinetically favourable on the flat and stepped surfaces, but hydrazine prefers to form NH_2 *via* N–N bond decoupling on the Cu(111) with an activation energy below 1 eV. The NH_2 molecule reacts fairly easily with co-adsorbed NH_2 to form NH_3 as well as with N_2H_x (x = 1–4) by abstracting hydrogen to produce NH_3 and N_2 molecules on both the flat and stepped surfaces. We also found that all intermediates except NNH prefer N–N bond breaking as the most likely dissociation pathway, where the amide and imide intermediates produced can be hydrogenated to form NH_3 in the presence of hydrogen. NNH is the only intermediate, which prefers to dissociate *via* a highly exothermic N–H bond breaking process to produce an N_2 molecule after overcoming a small barrier energy. We also studied the production of H_2 by recombination of hydrogen ad-atoms which, considering the activation energies, is particularly favoured under conditions of moderate temperatures. Our results agree well with experiments suggesting that N_2H_4 adsorbs dissociatively on copper above ~300 K leading to N_2, NH_3 and H_2. In general, the lower coordination of the steps is found to lead to higher reactivity than on the flat Cu(111) surface. Furthermore, the calculations show that the influence of step edge atoms is very different for the intra- and intermolecular dehydrogenation mechanisms. They also increase the barrier of N–N decoupling of all the existing species in the reaction.

Received 3rd June 2015,
Accepted 16th July 2015

DOI: 10.1039/c5cp03204k

www.rsc.org/pccp

1. Introduction

Hydrogen has received much attention over the last few decades as an energy resource,[1,2] for instance, in the proton exchange membrane (PEM) fuel cells which are some of the new carbon-free technologies for power generators. However, finding materials with a high storage capacity of hydrogen at room temperature is difficult and much effort is spent on developing new materials or employing organic and inorganic compounds for onboard hydrogen generation. Hydrazine (N_2H_4) with a hydrogen content of 12.5 wt% is a good hydrogen source for PEM fuel cells and since it is liquid at temperatures ranging from 2 °C to 114 °C, it is ideal for portable applications, for example for its current use in space vehicles or satellites.[3–5] Although hydrazine is a toxic substance, its decomposition products, N_2, H_2 and NH_3, are non-poisonous and carbon-free.[3] Its decomposition over catalysts at room temperature is exothermic without the need for external energy. Hydrazine is also used in a monopropellant thruster to control and adjust the orbits and altitudes of spacecrafts and satellites,[4,6] which is based on the production of larger volumes of N_2, H_2 and NH_3 gases from the decomposition of a relatively small volume of liquid hydrazine. The most important catalyst used for this reaction is Ir/Al_2O_3 with a high loading of iridium (20–40%).[4,6–8] However, due to the high price and limited resources of iridium, scientists are seeking to develop new, cheaper, active and readily available alternative catalysts for N_2H_4 decomposition.

We aim to investigate at the molecular level the catalytic activity of Cu towards N_2H_4 decomposition to understand the thermodynamics and kinetics of the elementary steps, and to evaluate if copper-based catalysts, which are much cheaper than iridium, could be used for hydrazine decomposition. Experimental studies have revealed that adsorption of N_2H_4 on copper at relatively low temperatures is likely to be reversible and non-dissociative up to ~300 K, above which hydrazine decomposes

[a] *Department of Chemistry, University College London, 20 Gordon Street, London, WC1H 0AJ, UK*
[b] *School of Chemistry, Cardiff University, Main Building, Park Place, Cardiff, CF10 3AT, UK. E-mail: DeLeeuwN@cardiff.ac.uk; Tel: +44 (0)2920870658*

and generates the gaseous products NH_3, N_2 and H_2.[9,10] There are two typical reactions for hydrazine decomposition;

$$N_2H_4 \rightarrow N_2 + 2H_2 \quad (1)$$

and

$$3N_2H_4 \rightarrow 4NH_3 + N_2 \quad (2)$$

The competition between the two decomposition reactions is influenced by the catalyst and the reaction conditions. A few comprehensive computational studies have been performed on the mechanism of hydrazine decomposition on transition metal surfaces, *e.g.* the density functional theory (DFT) study of hydrazine decomposition on the Ir(111) surface,[11] which showed that N–N bond cleavage of hydrazine is more easily accomplished than that of the N–H bond, and the NH_2 radicals can abstract hydrogen atoms one by one from N_2H_4 resulting in the formation of N_2 and NH_3 molecules. On Fe(211),[12] the dehydrogenation and nitrogen decoupling are competitive routes, with NH_2 and N being the dominant surface intermediates at mild temperatures, leading to gas-phase N_2 and NH_3 at higher temperatures. A DFT study of the dissociative adsorption of N_2H_4, by breaking of the hydrazine N–N bond, on low-index planar copper surfaces with and without Cu adatoms, showed that dissociative adsorption is thermodynamically strongly favoured over molecular sorption.[13] In this study, we have used improved DFT methodology, including long range interaction corrections to model more accurately the van der Waals forces, to analyse the thermodynamics and kinetics of the complete dissociation reaction.

Besides the more stable perfect and planar surfaces, defects and steps are common surface features. Previous experimental and theoretical results have suggested that low-coordinated sites show higher catalytic activity and can influence the overall surface chemistry.[14–20] Dahl *et al.*[21] showed that the energy barrier for N_2 dissociation is more than 1 eV lower on the Ru(0001) step edge than on the terraces. On the same surface, Zambelli *et al.*[22] have reported that the step edges are the active sites for NO dissociation. Xu and Mavrikakis showed that the tensile strain at steps substantially facilitates the O_2 activation on gold surfaces,[23] although the effect of steps on O_2 dissociation on Cu surfaces is not expected to be as pronounced as in other gas–metal systems.[24] The results for CO dissociation on the Ni surface indicate that the energy barriers for CO dissociation strongly favour reactions occurring near surface steps.[25] Fu and Somorjai[26] were able to provide evidence of the enhanced interaction of CO_2 on Cu steps, which results in the sensitivity of the methanol synthesis process to copper surface structures. Some studies have shown that the effect of step edge atoms is very different for the different reaction pathways. For example, Vang *et al.* in their study on ethylene dissociation on flat and stepped Ni(111) found that on the steps the barrier for C–C bond breaking is lowered significantly more than the barrier for dehydrogenation.

Following our investigation of the adsorption of molecular hydrazine on realistic Cu surfaces,[27–29] here we have carried out density functional theory calculations including dispersive interactions,[30,31] to characterize the most favourable adsorption sites, geometries and energies of the N_2H_4 decomposition intermediates. We have suggested and analysed three different decomposition mechanisms, including dehydrogenation *via* intra- and intermolecular pathways and N–N bond cleavage, on both flat and stepped Cu(111) surfaces.

2. Computational methods

We have carried out electronic structure calculations using DFT as implemented in the Vienna Ab initio Simulation Package (VASP).[32–35] The total energy calculations have been performed using the Perdew–Burke–Ernzerhof (PBE)[36] form of the generalized gradient approximation (GGA), whereas the projector augmented wave (PAW) method has been used to consider the effect of the inner cores on the valence density.[37,38] To improve the description of the long-range interaction, and following our previous work on the Cu–hydrazine system,[27] we have employed the DFT-D2 method of Grimme as implemented in VASP,[31] which has been shown to improve accuracy on several systems, *e.g.* ref. 27, 39 and 40. We have used the standard global scaling factor for the PBE functional within a damping function to avoid near singularities at small distances. We have also tested the DFT-D3 method to evaluate its effects on the adsorption energies compared to the DFT-D2 calculations. In line with Almora-Barrios *et al.*,[41] we found that the use of DFT-D3 led to larger binding energies, but also a more pronounced deviation from experimental values of the Cu lattice parameter and cohesive energy compared with those obtained by DFT-D2.[42] In this paper, we consider the energy differences between competing reactions to identify the preferred reaction mechanisms and pathways relative to each other, and as such DFT-D2 represents a sufficiently accurate model of the system to identify the reaction trends for hydrazine dissociation on the Cu surface.

Plane wave basis sets were used with an energy cut-off of 600 eV, which gave bulk energies converged to within 0.001 eV per atom. A $5 \times 5 \times 1$ and $3 \times 5 \times 1$ Monkhorst–Pack grid[43] of k points was used to sample the Brillouin zone for flat and stepped surfaces respectively. Spin polarization has been tested in a few cases but was found to be irrelevant.

The flat and stepped slabs were modelled with a 2×2 and 3×2 supercell from the full unit cell, $p(4 \times 4)$ and $p(6 \times 4)$, with 20 Å of vacuum between slabs in the z-direction where Cu–Cu distances were originally taken from the fully optimised bulk geometry. The adsorbate and the top three layers out of four and five layers of the flat and stepped slabs, respectively, were allowed to relax during structural optimisation, in line with previous studies.[44,45] Different slab thicknesses were tested until convergence was achieved within 0.01 eV per cell.

We have calculated the adsorption energies of the intermediates from the hydrazine decomposition process relative to the hydrazine molecule in the gas-phase:

$$E_{ads}(N_yH_x) = \left(E^{surf}_{N_yH_x} + (4-x)E^{surf}_{H} + (2-y)E^{surf}_{N}\right) - \left(((4-x)+(2-y)+1)E^{surf} + E^{gas}_{N_2H_4}\right) \quad (3)$$

Where $E^{surf}_{N_yH_x}$ is the total energy of the N_yH_x species adsorbed on a relaxed surface and E^{surf}_{H} and E^{surf}_{N} are the energies of an isolated H- and N-atom adsorbed somewhere else on the relaxed surface, at a non-interactive distance. E^{surf} and $E^{gas}_{N_2H_4}$ are the energies of the naked surface and isolated gas-phase hydrazine respectively. Within this definition, a negative E_{ads} value means a release of energy during adsorption. A combination of two varieties of the nudged elastic band (NEB) method[46,47] and the improved dimer method (IDM)[48] was used to identify transition state (TS) structures, which we verified by a single imaginary frequency associated with the reaction coordinate. The reaction energy (E_r) was obtained from the difference in energy between final and initial states and a negative E_r hence indicates an exothermic process. The forward and reverse activation barriers (E_a) were defined as the energy difference between the TS and the initial state or the final state, respectively.

3. Results

We have first created the perfect Cu(111) surface, which is the close-packed plane of the fcc structure (Fig. 1a) and is the most stable copper surface.[49] The surface Cu atoms are arranged in a hexagonal lattice with a separation of 2.52 Å between nearest neighbour atoms. The stepped Cu(111) surface has been studied to investigate the presence of an extended edge of low-coordinated atoms on the N_2H_4 dissociation behaviour (shown in Fig. 1b). Each unit cell in the stepped slab was offset by one atomic layer with respect to the next cell.[50–52]

The three major conformations of hydrazine in the gas-phase are *gauche*, *trans* and *eclipsed* (Fig. 2), where the *gauche* conformer is the lowest-energy structure. The *trans* and *eclipsed* conformations are 0.13 and 0.36 eV higher in energy, respectively, than the *gauche* conformation. We have identified the strongest adsorption geometries by placing the different intermediates at a variety of positions on the planar and stepped Cu(111) surfaces. Adsorption energies and structural parameters for various intermediate species in their most stable configurations on the flat and stepped Cu(111) are presented in Table 1 and Fig. 3. We note that because of the lower coordination of the stepped surface atoms, all intermediates are more stable on the step than on the terrace sites.

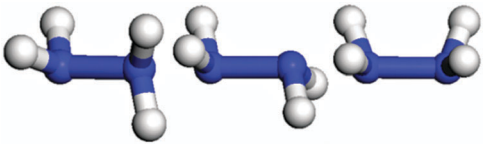

Fig. 2 Representation of the N_2H_4 conformations, from left to right: *gauche*, *trans* and *eclipsed*.

3.1 Adsorption on the planar and stepped Cu(111)

N_2H_4. We placed different N_2H_4 conformers (Fig. 2) in a number of non-equivalent initial configurations on the planar and stepped Cu(111) surface in order to identify the mode of strongest adsorption. The preferred N_2H_4 adsorption structures on the flat and stepped Cu(111) surfaces are in the *gauche* conformation, releasing an E_{ads} of 0.98 and 1.53 eV/N_2H_4 respectively. While it binds through both nitrogen atoms to the flat surface, η^2(N,N), with Cu–N distances of 2.178 Å, it prefers to bridge to the copper step edge atoms with shorter Cu–N distances of 2.104 Å. Hydrazine adsorbs almost parallel to both the flat and stepped surfaces, elongating the N–N bond to 1.452 and 1.455 Å respectively, compared to a length of 1.438 Å in the gas-phase. These configurations are a result of N–N bond rotation from *gauche* toward the *eclipsed* conformer with a torsional angle of 39.6° and 34.6° on the flat and stepped surfaces respectively.

N_2H_3. As the first product of dehydrogenation, the most stable adsorption structure for the N_2H_3 conformer is the $NHNH_2$ structure, which has different binding geometries on the flat *versus* the stepped Cu(111) surfaces: on the terrace, it prefers the hollow site with the NH-end closer to the surface, bridging two surface Cu atoms with a Cu–N bond length of ~2.0 Å, whereas the NH_2 part has a Cu–N bond length of 2.070 Å. On the step, it binds on the edge atoms with its NH-end inclined to the lower terrace, with a Cu–N distance of 2.078 Å. The N–N bond on the step edge elongates to 1.462 Å compared to 1.455 Å on the terrace. While the energy of N_2H_3 adsorption on the terrace is −0.85 eV relative to gas-phase hydrazine, it adsorbs more strongly to the step edge by 0.36 eV.

N_2H_2. The next intermediate is N_2H_2, which has two different conformers: NHNH, with one hydrogen atom at each nitrogen or NNH_2, where both hydrogen atoms are located on the same nitrogen. While the latter adsorbs perpendicularly on the

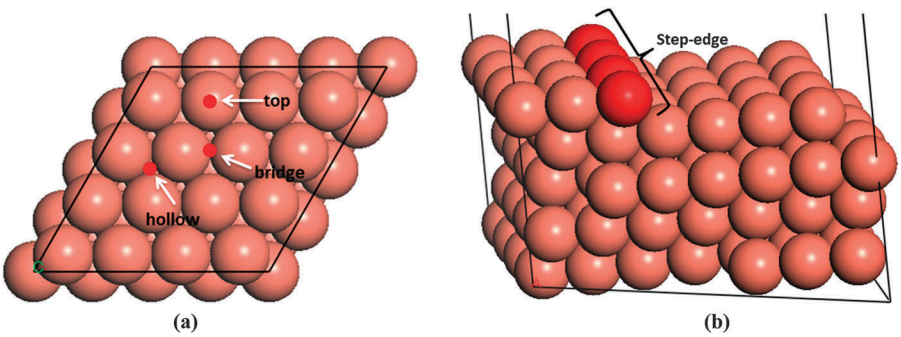

Fig. 1 The simulation cells and surface geometry of different sites used in the calculations of (a) perfect (top view) and (b) stepped (side view) surfaces. Note that low-coordinated atoms in the stepped surface are shaded darker.

Table 1 Adsorption energies (E_{ads}) and average geometric parameters of the most favourable adsorption structures of different N_2H_4 decomposition intermediates on the flat and stepped Cu(111) surface. Adsorption energies are relative to the gas-phase hydrazine; bold numbers show the adsorption energies relative to the species in their gas-phase: NH_3, N_2 and H_2

Adsorbate	E_{ads} (eV), flat	E_{ads} (eV), step	Cu–N (Å), flat	Cu–N (Å), step	N–N (Å), flat	N–N (Å), step	N–H (Å), flat	N–H (Å), step
N_2H_4	−0.98	−1.53	2.178	2.104	1.452	1.455	1.026	1.028
N_2H_3	−0.85	−1.21	2.023	2.033	1.455	1.462	1.024	1.027
NHNH	−0.10	−0.68	1.966	1.922	1.359	1.308	1.027	1.030
NNH_2	−0.18	−0.66	1.946	1.904	1.345	1.299	1.019	1.028
NNH	0.37	−0.39	1.971	1.938	1.240	1.237	1.041	1.042
NH_3	**−0.81**	**−1.06**	2.092	2.072	—	—	1.023	1.025
NH_2	−0.13	−1.42	1.982	1.942	—	—	1.021	1.022
NH	0.38	−0.58	1.898	1.566	—	—	1.022	1.023
N_2	**−0.15**	**−0.39**	1.985	1.931	1.121	1.123	—	—
H_2	**−0.10**	**−0.12**	—	—	—	—	—	—
N	**1.32**	**0.87**	1.838	2.002	—	—	—	—
H	**−0.28**	**−0.36**	—	—	—	—	—	—

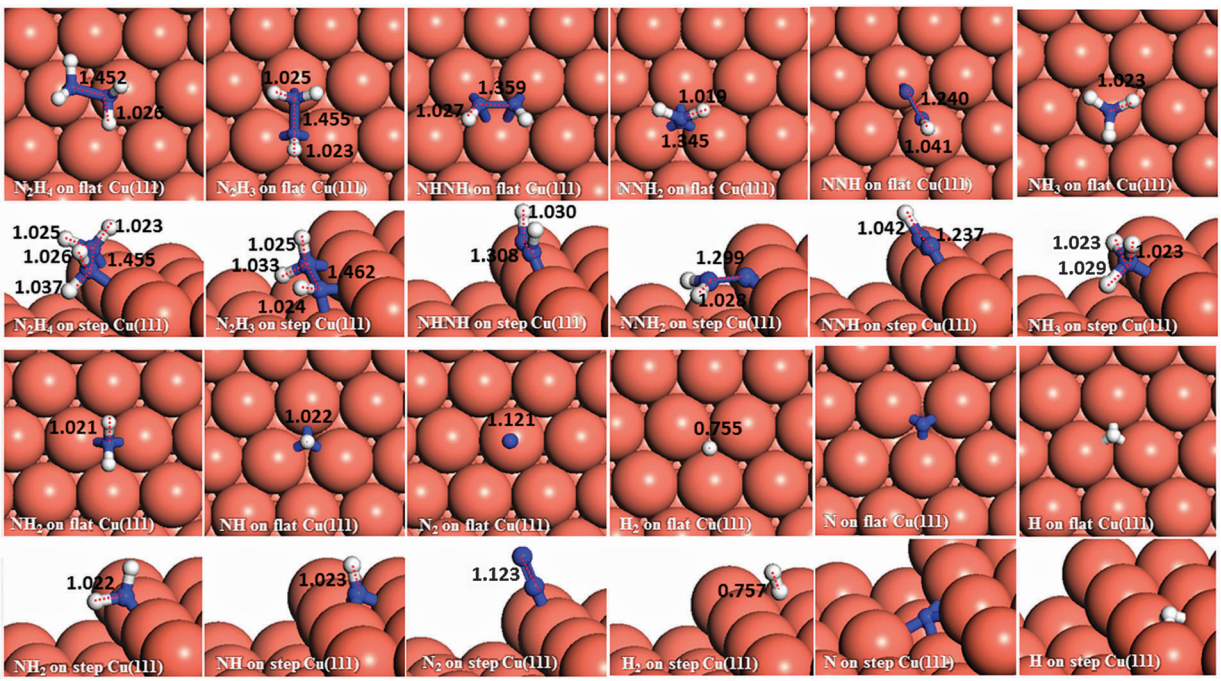

Fig. 3 Surface geometries of the preferred adsorption configurations of the various intermediates on the flat (top-view) and stepped (side-view) Cu(111) surfaces with their N–N and N–H bond distances in Å.

terrace with the lower N atom in a three-fold hollow site (E_{ads} = −0.18 eV), it prefers to bridge through the N on the step edge, lying parallel to the lower terrace with a larger adsorption energy of −0.66 eV. The adsorption of the NHNH structure on the terrace releases only 0.10 eV when it adsorbs through both nitrogen atoms in an hcp site parallel to the surface. NHNH bridges on the Cu step edges more strongly, releasing an energy of 0.68 eV.

N_2H. The adsorption geometries of N_2H are identical on both terrace and step surfaces, adsorbing on a bridge site through both nitrogen atoms parallel to the surface. While this process is endothermic (E_{ads} = 0.37 eV) on the terrace, the adsorption on the step edge is exothermic, releasing an energy of 0.39 eV. The N–N bond lengths on terrace and step edge are 1.240 and 1.237 Å respectively, *i.e.* elongated compared to 1.150 Å of the N_2H molecule in the gas-phase.[53]

N_2. We investigated the N_2 molecule adsorption at different sites on the surface and found that N_2 adsorbs on a top site on both the terrace or the step edge, with the molecule's axis perpendicular to the surface at Cu–N distances of 1.985 and 1.931 Å respectively. The N_2 adsorption energy with respect to gas-phase nitrogen is −0.15 and −0.39 eV on the flat and stepped surfaces respectively. It shows that nitrogen adsorption on the Cu surfaces is weak and it could easily desorb by increasing the temperature. The N–N bond length is 1.121 and 1.123 Å on the terrace and step edge respectively (an experimental bond length of 1.098 Å in the gas-phase[54]). In other sites, N_2 interacts more weakly and the molecule moves away to ∼3 Å from the surface.

N. The nitrogen atom adsorbs on a three-fold hollow site on the terrace and on a four-fold site at the foot of the step edge,

both endothermically requiring 1.32 and 0.87 eV on the terrace and step edge, respectively, relative to gas-phase N_2. This preference by N for a three-fold adsorption site on Cu(111) was also found in previous work.[55]

NH_3. The adsorption geometry of ammonia is identical on both the flat and stepped Cu surfaces with a preference for a top site, with Cu–N bond lengths of 2.092 and 2.072 Å on the flat and stepped surfaces respectively. Theoretical studies have shown that strong electrostatic contributions[56] and the Pauli repulsion of the lone-pair orbital of NH_3 by the copper 3d electrons[57] direct NH_3 towards one-fold adsorption on the copper surfaces. The NH_3 adsorption is exothermic with energies of −0.81 and −1.06 eV relative to gas-phase NH_3 on the terrace and step edge, respectively. These results show that the ammonia molecule adsorbs relatively strongly to the Cu surface and its desorption would be endothermic.

NH_2. The presence of low-coordinated Cu atoms stabilizes the NH_2 intermediates more than any other species, by increasing the NH_2 adsorption energy from −0.13 to −1.42 eV, while the adsorption geometry remains the same on both the terrace and step edge with NH_2 bridging between Cu surface atoms. The Cu–N bond and N–H bond lengths are 1.982 Å and 1.021 Å on the terrace and 1.942 Å and 1.022 Å on the step edge, which are slightly shorter than the experimentally reported N–H bond in the gas-phase (1.024 Å).[58]

NH. The adsorption of imide is endothermic by 0.38 eV on the flat Cu(111) surface, while on the stepped Cu(111) surface it is exothermic by 0.58 eV. The adsorption geometry for NH is identical on both the terrace and step edge, where it adsorbs on a three-fold hollow site, with a Cu–N bond length of 1.566 Å on the step edge compared to 1.898 Å on the flat surface.

H_2. The hydrogen molecule releases an energy of 0.10 eV relative to gas-phase hydrogen, when it is perpendicularly adsorbed on the fcc site of the terrace, with an H–H bond length of 0.755 Å (an experimental bond length of 0.741 Å in the gas-phase[54,58]). The adsorption on the step edge does not change the H_2 geometry on the Cu(111) surface, but makes it slightly more exothermic (E_{ads} = −0.12 eV) relative to gas-phase hydrogen. As such, hydrogen is physisorbed to the Cu surfaces at a distance of ∼2.80 Å, indicating that it should easily desorb from the surface.

H. For the hydrogen atom, similar to the nitrogen atom, the three-fold hollow site is the preferred site at low coverage. The hydrogen adsorption on both the flat and stepped surfaces is exothermic relative to gas-phase hydrogen, by 0.28 and 0.36 eV, respectively.

3.2 N_2H_x (x = 1–4) decomposition pathways on the planar and stepped Cu(111)

3.2.1 N_2H_4 dissociation and dehydrogenation. Table 2 summarizes the energetics of the different reaction pathways on both planar and stepped Cu(111) surfaces. We started from the most stable geometry of hydrazine, where hydrazine bridges through both nitrogen atoms to the Cu surface atoms. The pathways for hydrazine N–N bond breaking on both flat and stepped surfaces, leading to NH_2 intermediates, are shown in Fig. 4a. The reaction is exothermic (0.87 eV) on the flat surface with an energy barrier of 0.86 eV. The presence of low-coordinated atoms in the step makes the N–N bond breaking process more exothermic, releasing an energy of 1.66 eV, although the energy barrier is increased by 0.04 eV. This indicates that although a stepped surface favours the N–N bond breaking thermodynamically, it does not modify the kinetics of the reaction.

Dehydrogenation of N_2H_4 was also investigated (Fig. 4b). The energy barrier for this path on the flat surface is 1.55 eV and the process is endothermic by 0.31 eV. The activation energy on the stepped surface decreases to 1.11 eV, but the process becomes less favourable thermodynamically (E_r = 0.74 eV).

These results indicate that on Cu(111), with or without surface steps, the N–N bond cleavage of hydrazine is energetically and kinetically preferred over its dehydrogenation, which is in line with a previous experimental study showing that N–H bond breaking requires more energy than N–N breaking.[59] From the charge density calculations in our previous work,[27] which shows the induced charge density on the Cu(111) surface upon N_2H_4 adsorption, it can be observed that more charge is accumulated between the N and H atoms of hydrazine than between the two N atoms, which agrees well with these energetic results.

3.2.2 N_2H_3 dissociation and dehydrogenation. The N_2H_3 decomposition may proceed by N–N or N–H breaking. Initially, transition and final states for the N–N scission are represented in Fig. 5a leading to NH and NH_2. While this process has an activation barrier of 1.06 eV and the reaction is exothermic by 0.30 eV on the flat surface, the barrier increases by 0.21 eV but the reaction becomes more exothermic (0.76 eV) on the stepped surface.

There are two distinct pathways for dehydrogenation of N_2H_3, respectively, shown in Fig. 5b and c. The one leading to NNH_2 and a H atom has a barrier and reaction energy of 1.53 and 0.74 eV, respectively, on the flat surface, and 1.77 and 0.75 eV on the step. The alternative dehydrogenation pathway leads to NHNH and H as products. The barrier for this endothermic process (E_r = 0.84 eV) is 1.61 eV on the flat surface, while the step decreases the barrier to 1.56 eV although it is still endothermic (E_r = 0.69 eV).

Although NHNH and NNH_2 are products of the dehydrogenation of N_2H_3 on the Cu(111) surface, the N–N bond breaking of N_2H_3 is energetically more favourable. Our results indicate that low-coordinated atoms make the N–N decoupling of N_2H_3 more feasible thermodynamically, although they do not affect the kinetics.

3.2.3 N_2H_2 dissociation and dehydrogenation. We have studied the processes of N–N and N–H breaking of two N_2H_2 conformations: NNH_2 and NHNH. The pathway for N–N bond breaking of the NNH_2 intermediate, yielding NH_2 and N, see Fig. 6a, has an activation barrier and a reaction energy of 1.42 and +0.13 eV respectively. When the stepped surface is considered the N–N breaking barrier increases by 0.1 eV and the process is 0.05 eV more endothermic compared to the terrace. The dehydrogenation process of NNH_2 leads to NNH and an H atom (Fig. 6b). For this process on the flat surface, the required energy is 1.35 eV and the products are 0.58 eV higher in energy than the reactants. On the stepped surface, the barrier energy

Table 2 Calculated reaction (E_r) and barrier (E_a) energies for the forward and reverse reaction pathways considered. Note that (*) indicates the adsorbed state. E_r values of the adsorption and desorption processes are the corresponding E_{ads} values which for each species were calculated relative to the gas-phase

		Flat			Step		
	Reactions	E_r (eV)	E_a forward (eV)	E_a reverse (eV)	E_r (eV)	E_a forward (eV)	E_a reverse (eV)
Adsorption–desorption							
R1	$N_2H_4 \leftrightarrow N_2H_4$*	−0.98	—	—	−1.53	—	—
R2	NH_3* $\leftrightarrow NH_3$	0.81	—	—	1.06	—	—
R3	N_2* $\leftrightarrow N_2$	0.15	—	—	0.39	—	—
R4	H_2* $\leftrightarrow H_2$	0.10	—	—	0.12	—	—
N_2H_4 dissociation							
R5	N_2H_4* $\leftrightarrow 2NH_2$*	−0.87	0.86	1.73	−1.66	0.90	2.56
R6	N_2H_4* $\leftrightarrow N_2H_3$* + H*	0.31	1.55	1.24	0.74	1.11	0.37
N_2H_3 dissociation							
R7	N_2H_3* $\leftrightarrow NH_2$* + NH*	−0.30	1.06	1.36	−0.76	1.27	2.03
R8	N_2H_3* $\leftrightarrow NNH_2$* + H*	0.74	1.53	0.79	0.75	1.77	1.02
R9	N_2H_3* $\leftrightarrow$ NHNH* + H*	0.84	1.61	0.77	0.69	1.56	0.87
N_2H_2 dissociation							
R10	NNH_2* $\leftrightarrow NH_2$* + N*	0.13	1.42	1.29	0.18	1.52	1.34
R11	NHNH* $\leftrightarrow$ 2NH*	−0.34	0.85	1.19	−0.76	0.93	1.69
R12	NNH_2* $\leftrightarrow$ NNH* + H*	0.58	1.35	0.77	0.86	0.89	0.03
R13	NHNH* $\leftrightarrow$ NNH* + H*	0.60	1.68	1.08	0.43	1.39	0.96
NNH dissociation							
R14	NNH* $\leftrightarrow$ NH* + N*	0.16	1.47	1.31	−0.41	1.89	2.30
R15	NNH* $\leftrightarrow N_2$* + H*	−1.50	0.37	1.87	−1.11	0.62	1.73
N_2 dissociation							
R16	N_2* $\leftrightarrow$ 2N*	3.22	4.78	1.56	1.96	6.02	4.06
H–H coupling							
R17	2H* $\leftrightarrow H_2$*	0.43	1.08	0.65	0.81	1.28	0.47
NH_x (x = 1–3) dehydrogenation							
R18	NH_3* $\leftrightarrow NH_2$* + H*	0.74	1.63	0.89	0.67	1.59	0.92
R19	NH_2* $\leftrightarrow$ NH* + H*	0.67	1.59	0.92	1.06	1.81	0.75
R20	NH* $\leftrightarrow$ N* + H*	1.46	1.97	0.51	1.36	2.07	0.71
Interaction of NH_2 molecules							
R21	$2NH_2$* $\leftrightarrow$ NH* + NH_3*	−0.05	0.55	0.60	0.37	2.05	1.68
Interaction of NH_2 with N_2H_x (x = 1–4)							
R22	N_2H_4* + NH_2* $\leftrightarrow N_2H_3$* + NH_3*	−0.35	0.59	0.94	−0.22	0.03	0.25
R23	N_2H_3* + NH_2* $\leftrightarrow$ NHNH* + NH_3*	0.11	0.80	0.69	−0.01	0.64	0.65
R24	N_2H_3* + NH_2* $\leftrightarrow$ NNH_2* + NH_3*	−0.12	0.70	0.82	−0.06	0.67	0.73
R25	NNH_2* + NH_2* $\leftrightarrow$ NNH* + NH_3*	0.15	0.44	0.29	−0.47	0.15	0.62
R26	NHNH* + NH_2* $\leftrightarrow$ NNH* + NH_3*	−0.26	0.36	0.62	0.01	1.00	0.99
R27	NNH* + NH_2* $\leftrightarrow N_2$* + NH_3*	−2.13	0.14	2.29	−1.60	0.57	2.17

decreases to 0.89 eV but the process is more endothermic by 0.28 eV.

As to N–N bond breaking of NHNH (Fig. 7a), while the reaction barrier is 0.85 eV and the reaction is exothermic by −0.34 eV on the flat surface, these values increase to 0.93 and −0.76 eV, respectively, on the atomic step system. However, the dehydrogenation of NHNH resulting in NNH and an H species has a barrier of 1.68 eV and is endothermic by 0.60 eV on the flat surface (Fig. 7b). The lower coordination of the steps decreases both the barrier and the reaction energy to 1.39 and 0.43 eV respectively. Thus, the production of NH molecules *via* N–N bond breaking of NHNH is more favourable than other dissociation mechanisms of N_2H_2 from both thermodynamic and kinetic points of view.

3.2.4 NNH dissociation and dehydrogenation. Schematic representation of the NNH dissociation on the Cu(111) terrace is shown in Fig. 8a, where breaking the N–N bond leads to NH and N. The process has to overcome an energy barrier of 1.47 eV and it is slightly endothermic (E_r = 0.16 eV). The step edge makes the process more favourable thermodynamically with an exothermic reaction energy of −0.41 eV, but the energy barrier increases to 1.89 eV, making it therefore less feasible kinetically. The dehydrogenation reaction of NNH, which completes the dehydrogenation process of N_2H_4, is represented in Fig. 8b. This reaction pathway has energy barriers of 0.37 and 0.62 eV and is highly exothermic by −1.50 eV and −1.11 eV on the terrace and the step edge, respectively, which therefore becomes the most feasible intramolecular dehydrogenation reaction of any intermediate on the Cu(111) surface.

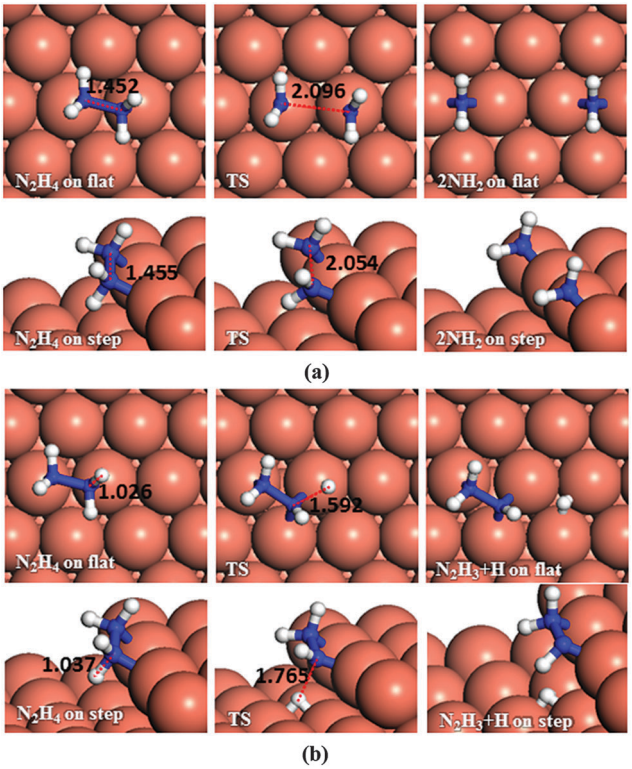

Fig. 4 Schematic representation of the initial, transition and final states for N_2H_4 dissociation pathways on the flat (top-view) and stepped (side-view) Cu(111) surfaces *via* (a) N–N, (b) N–H breaking. Bond lengths are given in Å.

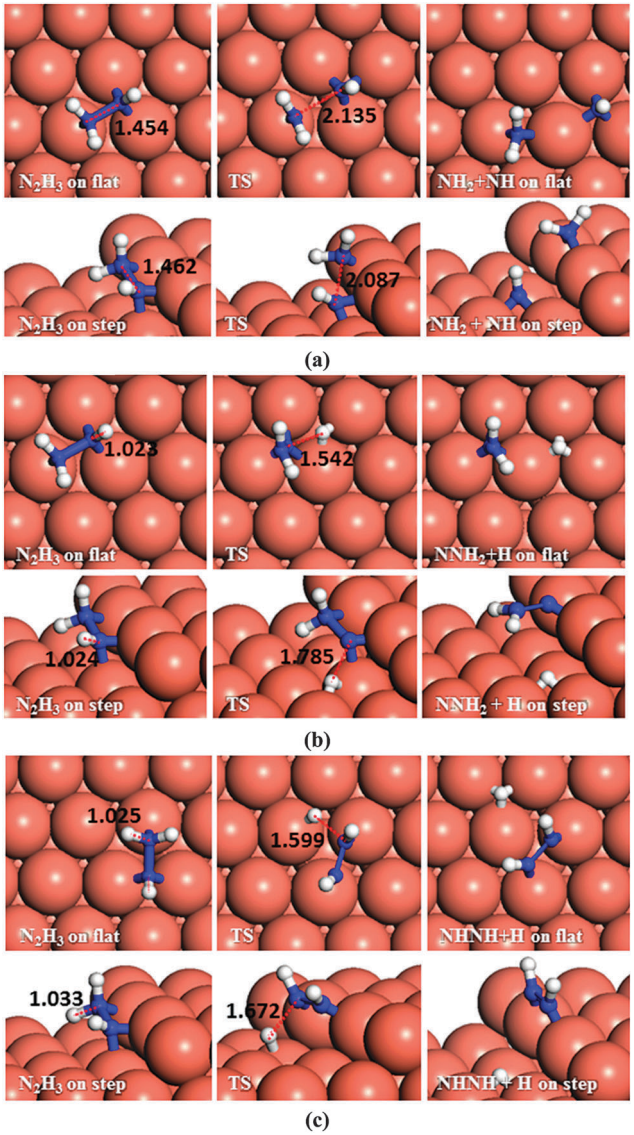

Fig. 5 Schematic representation of the initial, transition and final states for N_2H_3 dissociation pathways on the flat (top-view) and stepped (side-view) Cu(111) surfaces *via* (a) N–N, (b) and (c) N–H breaking. Bond lengths are given in Å.

3.2.5 N_2 dissociation. We have also considered the reaction pathway for N–N decoupling in the N_2 molecule on Cu(111) surfaces (Fig. 9). As expected, due to the molecule's strong interatomic bond, the process is highly unaffordable with energy barriers of 4.78 eV on the terrace and 6.02 eV on the step edge. The process is also highly endothermic (E_r = 3.22 eV) on the terrace, although the step reduces the endothermic reaction energy to 1.96 eV.

3.3 NH_x (x = 1–3) dehydrogenation

We have also investigated the consecutive dehydrogenation of ammonia, see Fig. 10a. The barrier and the endothermic reaction energy associated with the first N–H bond breaking process are 1.63 eV and 0.74 eV, respectively, on the flat surface, *i.e.* slightly higher than the barrier of 1.59 eV and a reaction energy of 0.67 eV on the step. The exothermic reverse (hydrogenation) reaction is more likely to happen with energy barriers of 0.89 and 0.92 eV on the terrace and step respectively. The dehydrogenation of NH_2 (Fig. 10b) and further dehydrogenation of NH (Fig. 10c) are also unlikely to succeed based on their associated high barrier energies, *i.e.* 1.59 and 1.97 eV on the flat surface and 1.81 and 2.07 on the stepped surface, respectively. The DFT calculated barrier energies for the dehydrogenation of NH_3, NH_2 and NH to form HCN on Pt(111) are smaller than our results, *i.e.* 1.39, 1.30 and 1.40 eV respectively,[60] although not significantly.

The reverse process, hydrogenation of NH has activation energies of 0.92 and 0.75 eV on the terrace and step, respectively. The hydrogenation of N is energetically favourable (E_r = −1.46 and −1.36 eV) leading to NH *via* energy barriers of only 0.51 and 0.71 eV on the flat and stepped surfaces, respectively. These energies show that the Cu surface could be a good catalyst for ammonia synthesis compared to the Ru(0001) surface, where the calculated barriers for hydrogenation of N, NH and NH_2 were found to be more than 1.2 and 1.1 eV on terraces and steps, respectively.[61,62]

3.4 H–H coupling

We have also considered another secondary process, the pathways for H–H coupling, see Fig. 11. As Table 2 shows, combining two hydrogen atoms on the stepped surface exhibits higher barrier and endothermic reaction energies of 1.28 and 0.81 eV than on

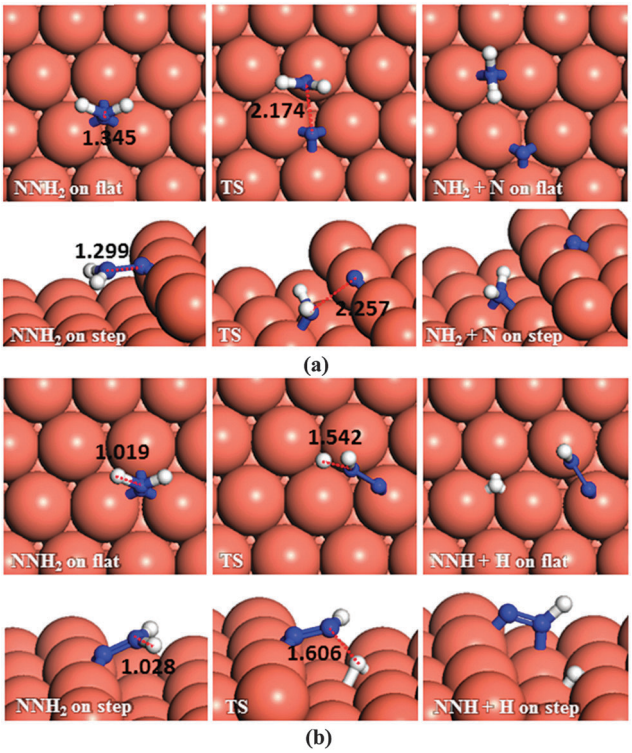

Fig. 6 Schematic representation of the initial, transition and final states for NNH_2 dissociation pathways on the flat (top-view) and stepped (side-view) Cu(111) surfaces *via* (a) N–N, and (b) N–H breaking. Bond lengths are given in Å.

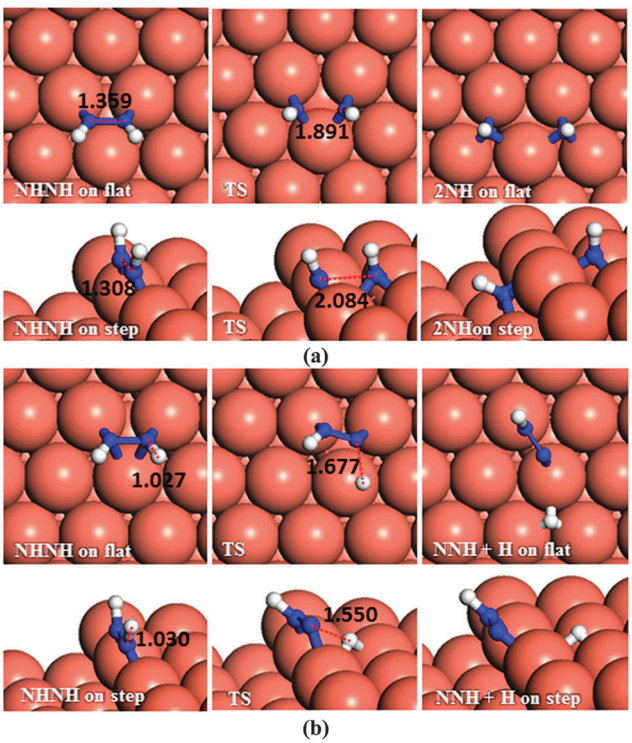

Fig. 7 Schematic representation of the initial, transition and final states for NNHNH dissociation pathways on the flat (top-view) and stepped (side-view) Cu(111) surfaces *via* (a) N–N, and (b) N–H breaking. Bond lengths are given in Å.

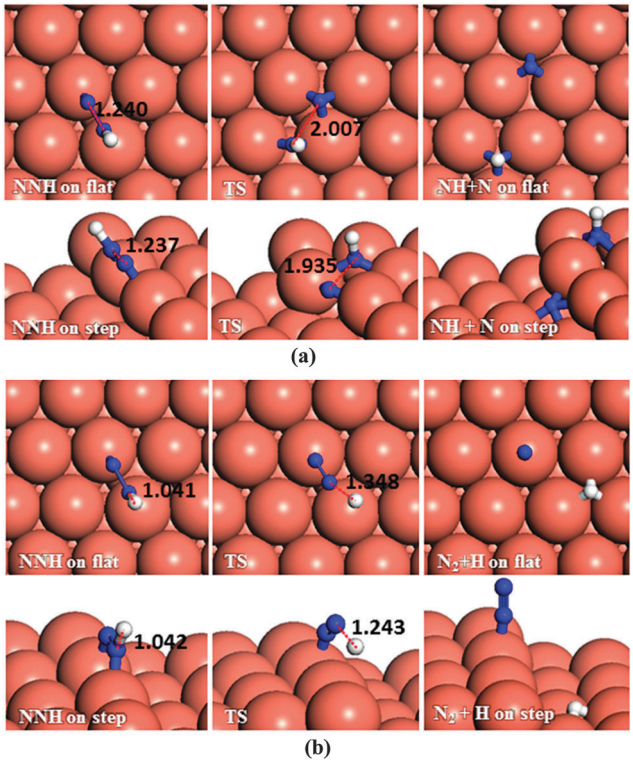

Fig. 8 Schematic representation of the initial, transition and final states for NNH dissociation pathways on the flat (top-view) and stepped (side-view) Cu(111) surfaces *via* (a) N–N, (b) N–H breaking. Bond lengths are given in Å.

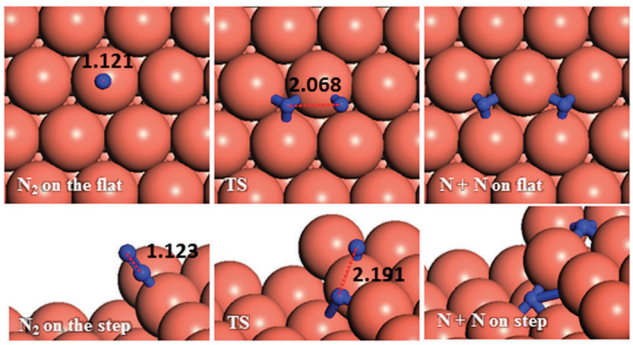

Fig. 9 Schematic representation of the initial, transition and final states for N_2 dissociation pathways on the flat (top-view) and stepped (side-view) Cu(111) surfaces. Bond lengths are given in Å.

the flat surface, E_a = 1.08 and E_r = 0.43 eV. The reverse reaction, the exothermic H_2 dissociation reaction, has energy barriers of 0.65 and 0.47 eV on the terrace and stepped surfaces, respectively, indicating that H_2 should adsorb dissociatively on Cu surfaces and the presence of a step edge makes this process more likely to proceed, due to the stabilisation provided by the low-coordinated atoms, where the electronic structure is different than that for the terrace atoms.[27,28]

3.5 Intermolecular dehydrogenation pathways

Having investigated the barriers for both N–N and N–H bond scission of the different possible intermediates of N_2H_4

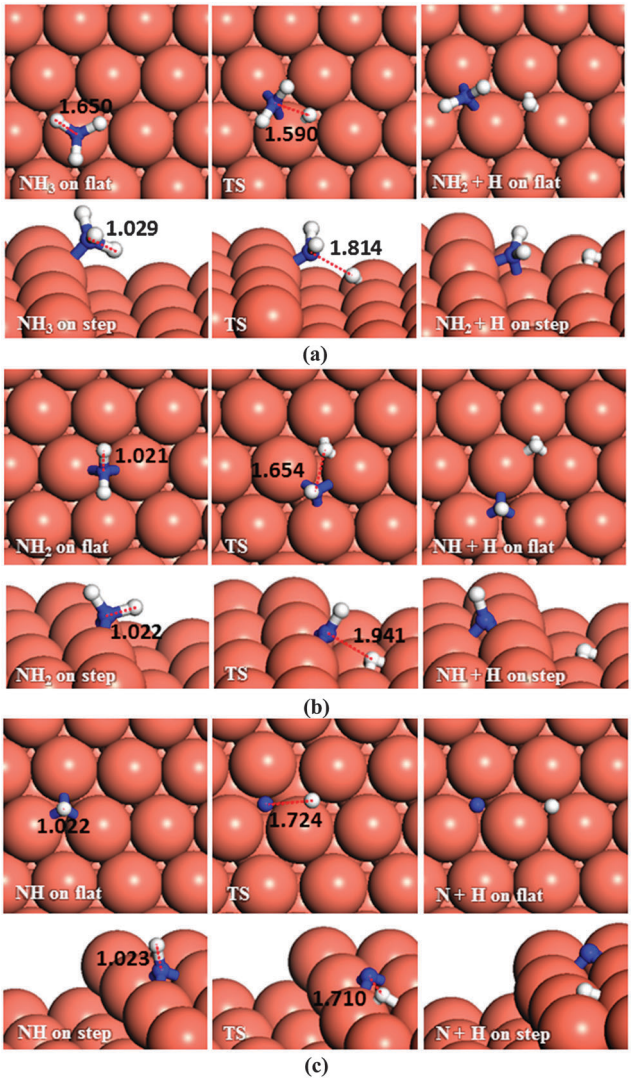

Fig. 10 Schematic representation of the initial, transition and final states for (a) NH_3, (b) NH_2 and (c) NH dehydrogenation pathways on the flat (top-view) and stepped (side-view) Cu(111) surfaces. Bond lengths are given in Å.

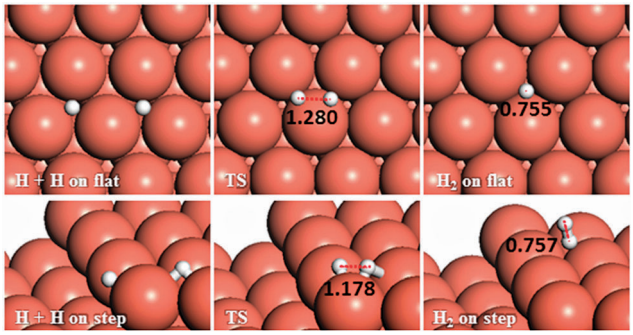

Fig. 11 Schematic representation of the initial, transition and final states for H–H coupling pathways on the flat (top-view) and stepped (side-view) Cu(111) surfaces. Bond lengths are given in Å.

dissociation, it is evident that breaking the hydrazine N–N bond and producing NH_2 fragments is the most likely process to occur on both the flat and stepped Cu(111) surfaces. Furthermore, the dehydrogenation of NH_2 is unfavourable to proceed at low temperatures due to the high energy of the transition states. We have therefore investigated other pathways involving the NH_2 groups. There are two possibilities: NH_2 can either react with another N_2H_x (x = 1–4) intermediate and subtract a hydrogen, or react with another NH_2 from hydrazine decomposition.

3.5.1 N_2H_x (x = 1–4) dehydrogenation by NH_2. The intermediate NH_2 may interact with hydrazine or other decomposition intermediates, and the pathways for subsequent dehydrogenation steps are shown in Fig. 12.

In the first suggested process (Fig. 12a), NH_2 interacts with N_2H_4 and abstracts one of its H atoms leading to N_2H_3 and NH_3. The energy barrier for this process is 0.59 eV on the flat surface, but it decreases to only 0.03 eV on the stepped surface, and releases energies of 0.35 and 0.22 eV, respectively. This step therefore could proceed fairly easily on both the flat and stepped Cu(111) surfaces.

In the second process, represented in Fig. 12b and c, the NH_2 molecule subtracts a hydrogen from N_2H_3 leading to NNH_2 or NHNH. If NNH_2 is formed, the process requires overcoming a barrier of 0.70 eV, but the products are 0.12 eV more favourable than the reactants on the flat surface. The presence of steps on the surface leads to NNH_2 *via* a slightly lower barrier (E_a = 0.67 eV), but releasing only 0.06 eV. The alternative pathway, leading to NHNH, has barriers of 0.80 and 0.64 eV on the terrace and step, respectively, while the process is endothermic by 0.11 eV on the terrace and practically in thermodynamic equilibrium (E_r = −0.01 eV) on the stepped surface.

In the next dehydrogenation pathway (Fig. 12d and e), NH_2 reacts with either the NNH_2 or NHNH structure, leading to the formation of NNH. The dehydrogenation process starting with NNH_2 is endothermic by 0.15 eV with an energy barrier of 0.44 eV on the terrace, while on the stepped surface it has a barrier of only 0.15 eV and an exothermic reaction energy of 0.47 eV. However, the interaction between NHNH and NH_2 is exothermic by 0.26 with a barrier of only 0.36 eV on the flat surface which increases by 0.64 eV for a thermodynamically equilibrated reaction on the stepped surface (E_a = 1.00 and E_r = 0.01 eV). The reaction between NH_2 and NHNH is therefore likely to succeed on the flat surface, although the reaction between NNH_2 and NH_2 is more feasible on the stepped surface.

In the last dehydrogenation process, the reaction between NH_2 and NNH yields N_2 and NH_3 (Fig. 12f). This reaction is highly exothermic releasing energies of 2.13 and 1.60 eV on the flat and stepped surfaces, respectively, which may be used for the desorption of N_2 and NH_3, which requires energies of 0.15 and 0.81 eV on the flat and 0.39 and 1.06 eV on the stepped surfaces, respectively.

3.5.2 Interaction of NH_2 molecules. The NH_2 molecules, *i.e.* produced by hydrazine N–N bond scission, may also react together leading to NH and NH_3, see Fig. 13. The calculated energy barrier for this reaction is only 0.55 eV and the products are practically in thermodynamic equilibrium with the reactants (E_r = −0.05 eV) on the flat surface. Although this process is therefore feasible on the flat Cu(111) surface, it is rather

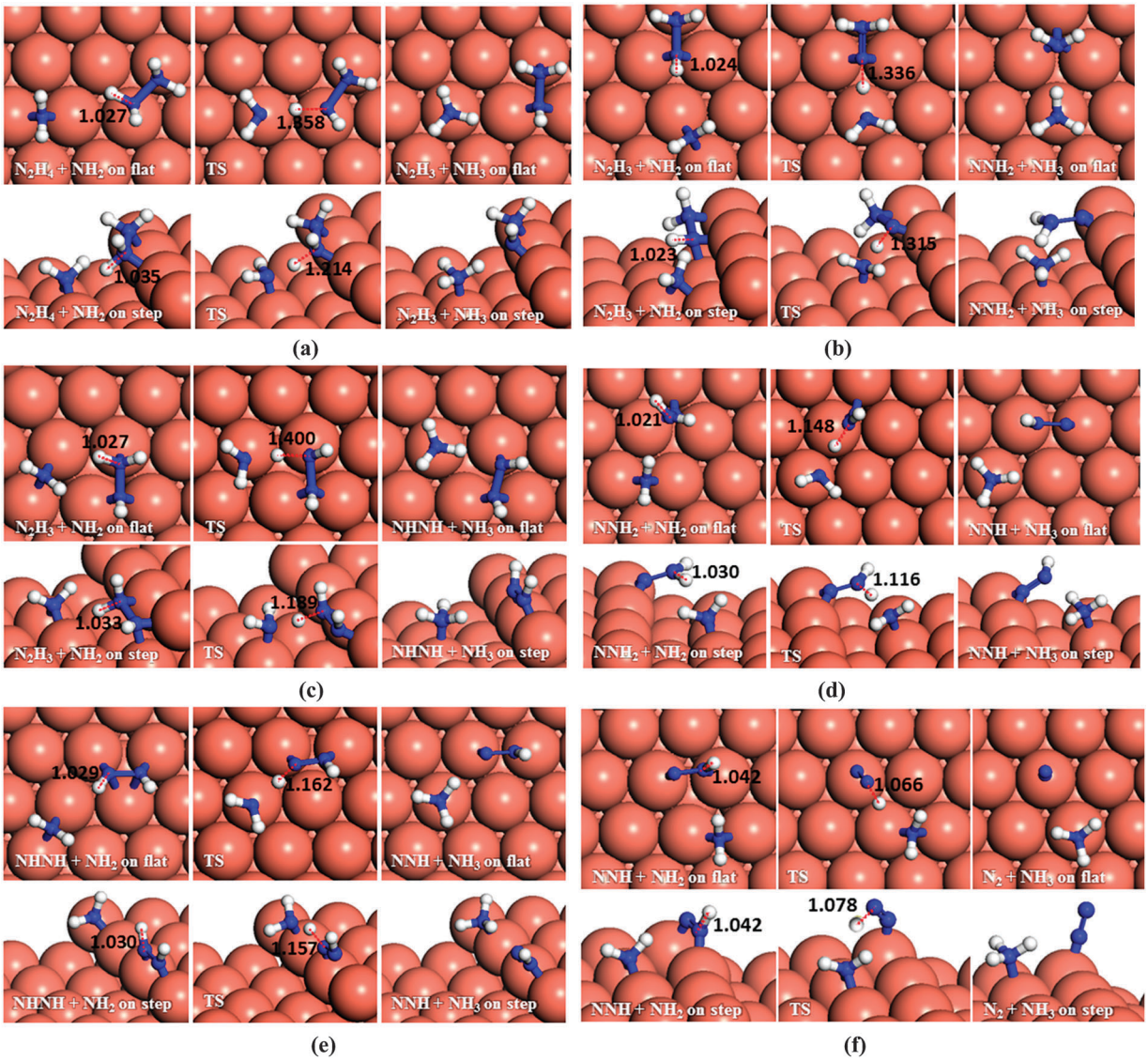

Fig. 12 Schematic representation of the initial, transition and final states for dehydrogenation pathways on the flat (top-view) and stepped (side-view) Cu(111) *via* NH_2 attacking to (a) N_2H_4, (b) and (c) N_2H_3, (d) NNH_2, (e) NHNH and (f) NNH. Bond lengths are given in Å.

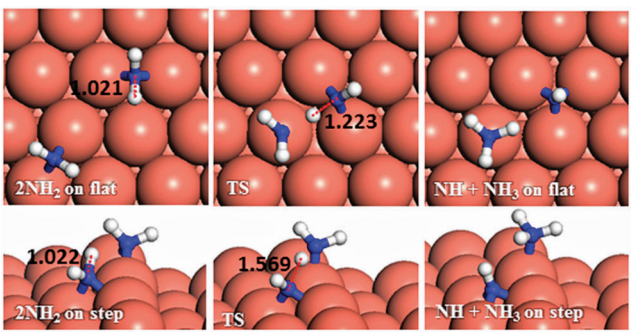

Fig. 13 Schematic representation of the initial, transition and final states for dehydrogenation pathways *via* NH_2 attacking NH_2 on the flat (top-view) and stepped (side-view) Cu(111) surfaces. Bond lengths are given in Å.

difficult to succeed on the stepped surface, due to a high barrier energy of 2.05 eV (E_r = 0.37 eV).

4. Discussion

The most stable adsorption structures of the dehydrogenation intermediates showed that their order of stability on the surface with respect to hydrazine is N_2H_4 > N_2H_3 > N_2H_2 > N_2H, indicating that more oxidised intermediates are less stable on the Cu surfaces. The same trend is found for the N–N average bond lengths, showing that dehydrogenation results in a shorter and stronger N–N bond and less stable intermediates on the surface.

We summarised the energy profiles of the reaction mechanism in Fig. 14–16. The plot in Fig. 14 contains the different pathways for intramolecular dehydrogenation, whereas the N_2H_4 decomposition *via* N–N scission and further dehydrogenation reactions are shown in Fig. 15 and Fig. 16 summarises the intermolecular dehydrogenation pathway.

The N_2H_4 dehydrogenation, $N_2H_4^* \rightarrow N_2H_3^* + H^*$, and subsequent ones are unlikely to occur under moderate conditions,

owing to the high reaction barriers, see Table 2 and Fig. 14. The rate-determining step for the N_2H_4 intramolecular dehydrogenation mechanism is NHNH* → NNH* + H* on the flat surface with an energy barrier of 1.68 eV, and N_2H_3* → NNH_2* + H* on the stepped surface with an activation barrier of 1.77 eV. It is therefore unlikely that a large amount of N_2 is produced *via* this intramolecular dehydrogenation pathway. Overall, from the investigation of N–H bond scission of all species on the surface, NNH is the only fragment which is easily dehydrogenated to the N_2 molecule, with barriers of only 0.37 and 0.62 eV on the flat and stepped surfaces, respectively, and a relatively exothermic reaction ($E_r \sim 1.3$ eV). These results also suggest that at moderate temperatures the recombination of produced H atoms will lead to the formation of H_2; this reaction has activation energies of ~1.1 eV on the flat and stepped surfaces and the products desorb easily from the surface.

From investigation of N–N bond scission in any intermediate on the surface, we found that the N–N decoupling in

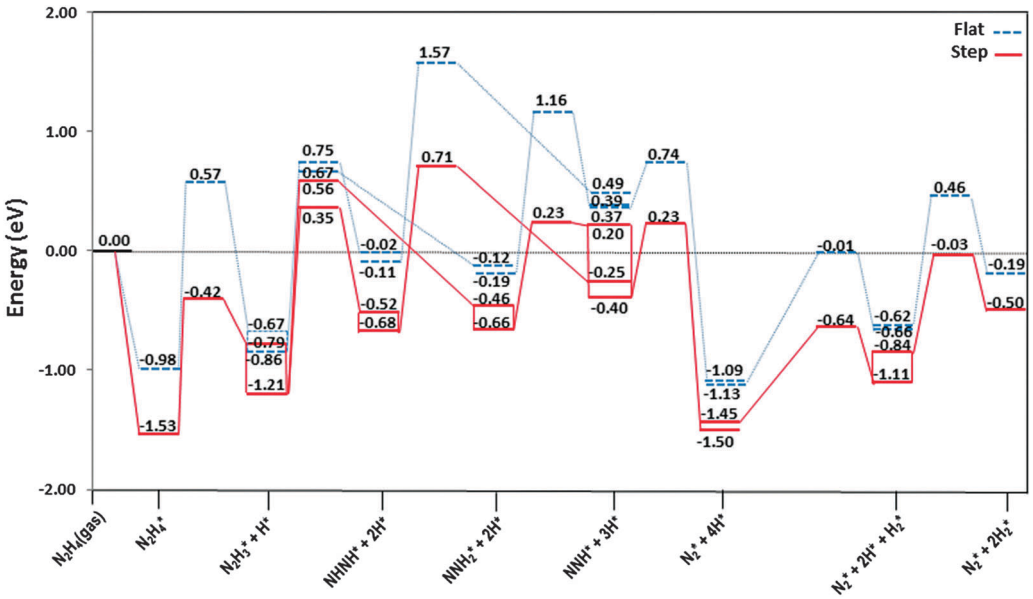

Fig. 14 Reaction profiles for dissociation of N_2H_4 *via* intramolecular dehydrogenation mechanism on the flat (---) and stepped (—) Cu(111) surfaces. Energies are relative to the energy of the gas-phase hydrazine (in eV). Note that we have considered the diffusion of intermediates to their most stable adsorption sites on the surface as a barrierless pathway.

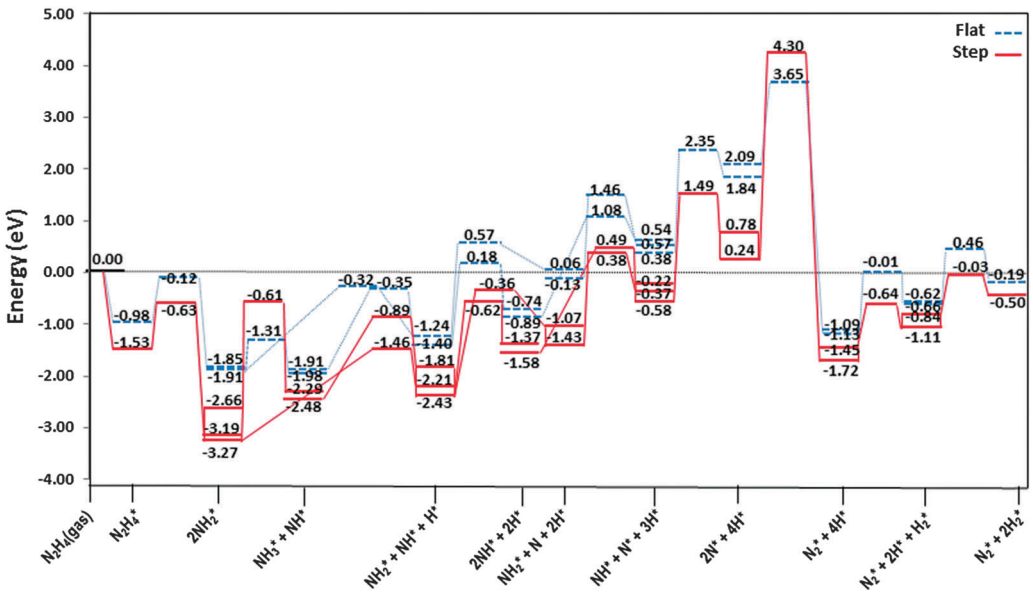

Fig. 15 Reaction profiles for dissociation of N_2H_4 *via* N–N bond breaking and subsequent dehydrogenation pathways on the flat (---) and stepped (—) Cu(111) surfaces. Energies are relative to the energy of the gas-phase hydrazine (in eV). Note that we have considered the diffusion of intermediates to their most stable adsorption sites on the surface as a barrierless pathway.

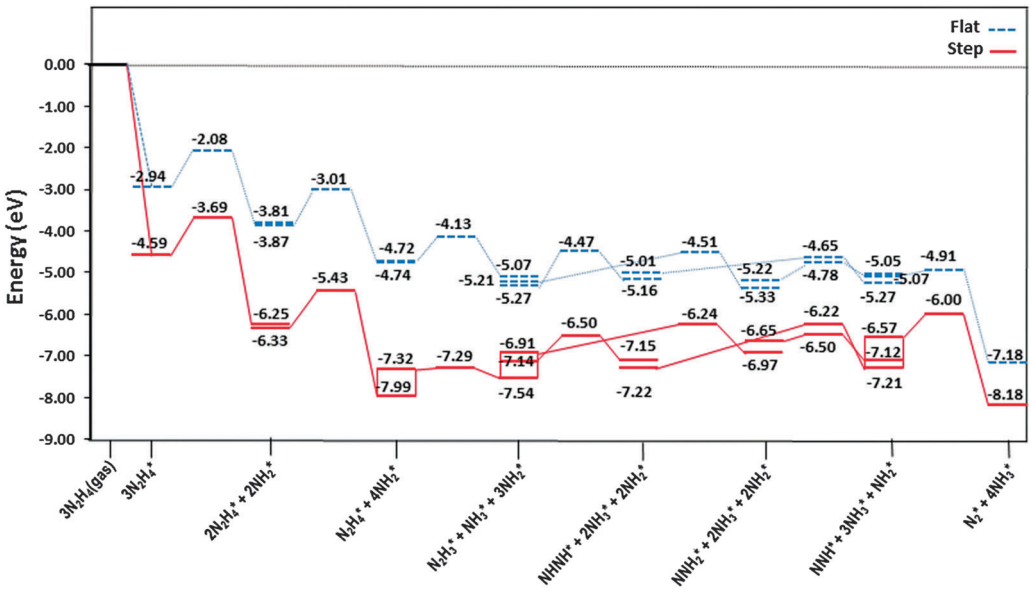

Fig. 16 Reaction profiles for dissociation of N_2H_4 *via* intermolecular dehydrogenation *via* NH_2 on the flat (---) and stepped (—) Cu(111) surfaces. Energies are relative to the energy of the gas-phase hydrazine (in eV). Note that we have considered the diffusion of intermediates to their most stable adsorption sites on the surface as a barrierless pathway.

N_2H_4 (N_2H_4* → $2NH_2$*), see Table 2 and Fig. 15, is the predominant mechanism, leading to amide intermediate production in agreement with experiment.[59] The exothermic decomposition of N_2H_3 and NHNH fragments *via* N–N decoupling also has low activation energies compared to the other intermediates on the flat and stepped surfaces.

The production of NH_3 takes place from the exothermic reaction of NH_2 radicals on the flat surface by an activation energy of only 0.55 eV. Further NH_3 production from the interaction of N_2H_x (x = 1–4) and NH_2 is also possible, resulting in the production of N_2; all these steps have barrier energies below 1 eV on either the flat or stepped surfaces, see Table 2 and Fig. 16. The rate-determining step for the intermolecular dehydrogenation *via* NH_2 is the reaction N_2H_3* + NH_2* → NHNH* + NH_3* which has an activation energy of 0.80 eV on the flat surface, while on the stepped surfaces NHNH* + NH_2* → NNH* + NH_3* has a barrier of 1.00 eV where it is the rate-determining step. The N_2 molecule produced from one single hydrazine molecule *via* an intermolecular dehydrogenation mechanism, Fig. 16, is in agreement with experimental reports where N_2H_4 remains stable during the dissociation process.[59,63]

Thus we may conclude that the NH_2 radical governs the N_2H_4 dissociation, which agrees well with experimental studies about the role of NH_2 in the hydrazine decomposition.[64,65] The released energies from the exothermic reactions provide enough energy for the evolution of NH_3, N_2 and H_2 gases from the surface. Experimental studies also revealed that the decomposition of hydrazine on copper films occurs above 300 K with gaseous products of NH_3, N_2 and some H_2,[10] which is consistent with the mechanism in Fig. 16.

Furthermore, the calculations showed the influence of low-coordinated atoms on the different N_2H_4 decomposition pathways, *i.e.* at the step edges. These surface atoms stabilise some intermediates more than others along the different pathways, although there is no clear trend in the activation energies except to increase the N–N decoupling barriers of the intermediates in the presence of step edge atoms.

5. Conclusions

We have employed DFT level calculations with long-range interaction corrections to carry out a systematic study of the N_2H_4 decomposition mechanisms on the flat and stepped Cu(111) surfaces. We have identified the most stable adsorption sites for all intermediates along the different mechanisms of N–H and N–N bond scission. We have found that N_2H_4 dehydrogenation is kinetically an unlikely process on both flat and stepped Cu(111) surfaces due to high barrier energies. However, N–N decoupling is energetically feasible, leading to NH_2 intermediates. The intermolecular dehydrogenation reaction is the predominant mechanism between either NH_2 fragments on the flat surface, or NH_2 and N_2H_x (x = 1–4) intermediates on the flat or stepped surfaces, leading to the formation of N_2 and NH_3, as shown in Fig. 16. This process is highly exothermic, releasing ~2.50 eV per hydrazine molecule, which agrees well with the use of N_2H_4 as a rocket fuel. Meanwhile the amide and imide intermediates are hydrogenated to NH_3 in the presence of hydrogen, which competes with the recombination of H atoms leading to H_2 molecules. We also found that, while the introduction of low-coordinated atoms, as on the step edge on the surface, increases the barrier of N–N decoupling along the reaction, it has different effects on the barriers of intra- and intermolecular dehydrogenation mechanisms.

Future work will include microkinetic simulations to develop our understanding of the competing catalytic processes leading to N_2H_4 dissociation on the planar Cu(111) surfaces.

Acknowledgements

S.S.T acknowledges University College London and the UCL Industrial Doctorate Centre in Molecular Modelling and Materials Science for an Overseas Research Scholarship. N.H.d.L acknowledges the Royal Society for an Industry Fellowship and A.R. is grateful to the Ramsay Memorial Trust and University College London for the award of a Ramsay Fellowship. *Via* our membership of the UK's HPC Materials Chemistry Consortium, which is funded by EPSRC (EP/L000202), this work made use of the facilities of HECToR and ARCHER, the UK's national high-performance computing service, which is funded by the Office of Science and Technology through EPSRC's High End Computing Programme, as well as the UCL Legion High Performance Computing facility (Legion@UCL), and associated support services, in the completion of this work.

References

1 S. Dutta, *J. Ind. Eng. Chem.*, 2014, **20**, 1148–1156.
2 L. Schlapbach and A. Zuttel, *Nature*, 2001, **414**, 353–358.
3 M. Y. Zheng, R. H. Cheng, X. W. Chen, N. Li, L. Li, X. D. Wang and T. Zhang, *Int. J. Hydrogen Energy*, 2005, **30**, 1081–1089.
4 E. W. Schmidt, *Hydrazine and Its Deratives: Preparation, Properties, Applications*, Wiley, New York, 2001.
5 S. G. Pakdehi, M. Salimi and M. Rasoolzadeh, *Researches and Applications in Mechanical Engineering*, 2014, **3**, 21–25.
6 S. Mary, C. Kappenstein, S. Balcon, S. Rossignol and E. Gengembre, *Appl. Catal., A*, 1999, **182**, 317–325.
7 S. Balcon, S. Mary, C. Kappenstein and E. Gengembre, *Appl. Catal., A*, 2000, **196**, 179–190.
8 J. P. Contour and G. Pannetie, *J. Catal.*, 1972, **24**, 434–445.
9 M. H. Matloob and M. W. Roberts, *J. Chem. Soc., Faraday Trans. 1*, 1977, **73**, 1393–1405.
10 Y. K. Alhaydari, J. M. Saleh and M. H. Matloob, *J. Phys. Chem.*, 1985, **89**, 3286–3290.
11 P. X. Zhang, Y. G. Wang, Y. Q. Huang, T. Zhang, G. S. Wu and J. Li, *Catal. Today*, 2011, **165**, 80–88.
12 H. L. McKay, S. J. Jenkins and D. J. Wales, *J. Phys. Chem. C*, 2011, **115**, 17812–17828.
13 T. D. Daff and N. H. de Leeuw, *J. Mater. Chem.*, 2012, **22**, 23210–23220.
14 J. K. Norskov, T. Bligaard, A. Logadottir, S. Bahn, L. B. Hansen, M. Bollinger, H. Bengaard, B. Hammer, Z. Sljivancanin, M. Mavrikakis, Y. Xu, S. Dahl and C. J. H. Jacobsen, *J. Catal.*, 2002, **209**, 275–278.
15 Z. P. Liu and P. Hu, *J. Am. Chem. Soc.*, 2003, **125**, 1958–1967.
16 T. Zubkov, G. A. Morgan, J. T. Yates, O. Kuhlert, M. Lisowski, R. Schillinger, D. Fick and H. J. Jansch, *Surf. Sci.*, 2003, **526**, 57–71.
17 P. Gambardella, Ž. Šljivančanin, B. Hammer, M. Blanc, K. Kuhnke and K. Kern, *Phys. Rev. Lett.*, 2001, **87**, 056103.
18 I. M. Ciobica and R. A. van Santen, *J. Phys. Chem. B*, 2002, **106**, 6200–6205.
19 N. H. de Leeuw and J. A. Purton, *Phys. Rev. B: Condens. Matter Mater. Phys.*, 2001, **63**, 195417.
20 S. C. Parker, N. H. de Leeuw, D. J. Harris, F. M. Higgins, P. M. Oliver, S. E. Redfern and G. W. Watson, *Radiat. Eff. Defects Solids*, 1999, **151**, 185–195.
21 S. Dahl, A. Logadottir, R. C. Egeberg, J. H. Larsen, I. Chorkendorff, E. Tornqvist and J. K. Norskov, *Phys. Rev. Lett.*, 1999, **83**, 1814–1817.
22 T. Zambelli, J. Wintterlin, J. Trost and G. Ertl, *Science*, 1996, **273**, 1688–1690.
23 Y. Xu and M. Mavrikakis, *J. Phys. Chem. B*, 2003, **107**, 9298–9307.
24 Y. Xu and M. Mavrikakis, *Surf. Sci.*, 2003, **538**, 219–232.
25 T. Li, B. Bhatia and D. S. Sholl, *J. Chem. Phys.*, 2004, **121**, 10241–10249.
26 S. S. Fu and G. A. Somorjai, *Surf. Sci.*, 1992, **262**, 68–76.
27 S. S. Tafreshi, A. Roldan, N. Y. Dzade and N. H. de Leeuw, *Surf. Sci.*, 2014, **622**, 1–8.
28 S. S. Tafreshi, A. Roldan and N. H. de Leeuw, *J. Phys. Chem. C*, 2014, **118**, 26103–26114.
29 S. S. Tafreshi, A. Roldan and N. H. de Leeuw, *Surf. Sci.*, 2015, **637–638**, 140–148.
30 S. Grimme, *J. Comput. Chem.*, 2004, **25**, 1463–1473.
31 S. Grimme, *J. Comput. Chem.*, 2006, **27**, 1787–1799.
32 G. Kresse and J. Furthmuller, *Phys. Rev. B: Condens. Matter Mater. Phys.*, 1996, **54**, 11169–11186.
33 G. Kresse and J. Furthmuller, *Comput. Mater. Sci.*, 1996, **6**, 15–50.
34 G. Kresse and J. Hafner, *Phys. Rev. B: Condens. Matter Mater. Phys.*, 1993, **47**, 558–561.
35 G. Kresse and J. Hafner, *Phys. Rev. B: Condens. Matter Mater. Phys.*, 1994, **49**, 14251–14269.
36 J. P. Perdew, K. Burke and M. Ernzerhof, *Phys. Rev. Lett.*, 1996, **77**, 3865–3868.
37 G. Kresse and D. Joubert, *Phys. Rev. B: Condens. Matter Mater. Phys.*, 1999, **59**, 1758–1775.
38 P. E. Blochl, *Phys. Rev. B: Condens. Matter Mater. Phys.*, 1994, **50**, 17953–17979.
39 S. Irrera, A. Roldan, G. Portalone and N. H. De Leeuw, *J. Phys. Chem. C*, 2013, **117**, 3949–3957.
40 N. Y. Dzade, A. Roldan and N. H. de Leeuw, *J. Chem. Phys.*, 2013, **139**, 124708.
41 N. Almora-Barrios, G. Carchini, P. Blonski and N. Lopez, *J. Chem. Theory Comput.*, 2014, **10**, 5002–5009.
42 W. Reckien, F. Janetzko, M. F. Peintinger and T. Bredow, *J. Comput. Chem.*, 2012, **33**, 2023–2031.
43 H. J. Monkhorst and J. D. Pack, *Phys. Rev. B: Solid State*, 1976, **13**, 5188–5192.
44 R. Koitz, A. P. Seitsonen, M. Iannuzzi and J. Hutter, *Nanoscale*, 2013, **5**, 5589–5595.
45 M. Gajdos and J. Hafner, *Surf. Sci.*, 2005, **590**, 117–126.
46 G. Mills and H. Jonsson, *Phys. Rev. Lett.*, 1994, **72**, 1124–1127.
47 G. Mills, H. Jonsson and G. K. Schenter, *Surf. Sci.*, 1995, **324**, 305–337.
48 A. Heyden, A. T. Bell and F. J. Keil, *J. Chem. Phys.*, 2005, **123**, 224101.

49 T. D. Daff, D. Costa, I. Lisiecki and N. H. de Leeuw, *J. Phys. Chem. C*, 2009, **113**, 15714–15722.
50 N. H. de Leeuw, S. C. Parker, C. R. A. Catlow and G. D. Price, *Am. Mineral.*, 2000, **85**, 1143–1154.
51 N. H. de Leeuw and C. J. Nelson, *J. Phys. Chem. B*, 2003, **107**, 3528–3534.
52 N. H. de Leeuw, C. J. Nelson, C. R. A. Catlow, P. Sautet and W. Dong, *Phys. Rev. B: Condens. Matter Mater. Phys.*, 2004, **69**, 045419.
53 J. A. Pople and L. A. Curtiss, *J. Chem. Phys.*, 1991, **95**, 4385–4388.
54 K. P. Huber and G. Herzberg, *Molecular Spectra and Molecular Structure: IV. Constants of Diatomic Molecules*, Van Nostrand Reinhold Company, New York, 1979.
55 G. C. Wang, L. Jiang, X. Y. Pang and J. Nakamura, *J. Phys. Chem. B*, 2005, **109**, 17943–17950.
56 W. Biemolt, P. R. Davies, A. P. J. Jansen and R. A. Vansanten, *Catal. Today*, 1992, **12**, 427–432.
57 W. Biemolt, G. J. C. S. Vandekerkhof, P. R. Davies, A. P. J. Jansen and R. A. Vansanten, *Chem. Phys. Lett.*, 1992, **188**, 477–486.
58 D. R. Lide, *CRC Handbook of Cemistry and Physics*, CRC Press, New York, 1996.
59 J. Block and G. Schulzek, *J. Catal.*, 1973, **30**, 327–329.
60 J. Gomez-Diaz and N. Lopez, *J. Phys. Chem. C*, 2011, **115**, 5667–5674.
61 A. Logadottir and J. K. Norskov, *J. Catal.*, 2003, **220**, 273–279.
62 K. Honkala, A. Hellman, I. N. Remediakis, A. Logadottir, A. Carlsson, S. Dahl, C. H. Christensen and J. K. Norskov, *Science*, 2005, **307**, 555–558.
63 R. Maurel and J. C. Menezo, *J. Catal.*, 1978, **51**, 293–295.
64 K. I. Aika, T. Ohhata and A. Ozaki, *J. Catal.*, 1970, **19**, 140.
65 A. A. Konnov and J. De Ruyck, *Combust. Flame*, 2001, **124**, 106–126.

